

# Fabrication of High-Quality Thin Single-Crystal Diamond Membranes with Low Surface Roughness

Julia Heupel,\* Maximillian Pallmann, Jonathan Körber, David Hunger, Johann Peter Reithmaier, and Cyril Popov

Certain aspects before and during the fabrication of single-crystal diamond (SCD) membranes are highlighted, which are decisive to obtain high-quality membranes with low surface roughness values around 0.2 nm on a small area scale. In addition to the requirements for the starting material, including a high planarity and a moderate surface roughness, the importance of cleaning processes to minimize particles and impurities before and during the structuring is emphasized. With the help of a planarization procedure, consisting of a combination of different Ar/Cl<sub>2</sub> recipes with low etch rates, surface defects like grooves due to polishing are minimized and smooth surfaces are acquired. Severe micro-masking can be prevented by the application of a cyclic Ar/Cl<sub>2</sub> + O<sub>2</sub> recipe, allowing finally the fabrication of defect-minimized and planarized SCD membranes in the thickness range between a few microns and a few hundred nanometers. The high quality of the structured SCD membranes is evidenced with a morphological as well as optical characterization via fiber-based microcavity measurements.

## 1. Introduction

Single-crystal diamond (SCD) in particular in form of thin membranes<sup>[1–3]</sup> has gained an ever-increasing scientific interest over the years based on diamond's exceptional optical<sup>[4,5]</sup> and electrical<sup>[6,7]</sup> properties. Therefore, it has emerged as a highly promising platform e.g., in the field of nanophotonics for photonic integrated devices<sup>[8–10]</sup> and envisioned applications in quantum information technologies (QITs), such as quantum memories<sup>[11,12]</sup> and quantum communication.<sup>[13,14]</sup> Different kinds of optically active point defects in the SCD lattice, the so-called color centers like the nitrogen-vacancy (NV) center<sup>[15,16]</sup> or the silicon-vacancy (SiV) center,<sup>[17,18]</sup> show favorable characteristics, e.g., high photostability at room temperature and practica-

ble control of coherent single spins, to serve as single-photon emitters in QITs.


However, due to the high refractive index of diamond ( $n_d \approx 2.41$ )<sup>[19]</sup> inducing total internal reflection at the diamond–air interface, light-confining architectures like nanopillars,<sup>[20,21]</sup> solid immersion lenses,<sup>[22,23]</sup> photonic crystal cavities<sup>[24,25]</sup> or Fabry–Pérot microcavities<sup>[26]</sup> are necessary to yield an efficient outcoupling from the zero-phonon line (ZPL) of the color centers and to improve the photon collection efficiency. For a strong and selective Purcell enhancement of the ZPL, cavities with a small mode volume and high-quality factor are required. One promising approach is the introduction of thin diamond membranes in fiber-based microcavities.<sup>[3,27]</sup> While such microcavities allow for spatial and spectral tunability as well as a direct outcoupling of photons in a single-mode fiber, the system efficiency can be limited by additional losses introduced by the diamond itself. Here the most crucial parameter is the surface roughness of the SCD membrane leading to scattering at the diamond–air interface.<sup>[28,29]</sup> For an effective Purcell enhancement and to maintain a high finesse, the membrane should be a few micrometers thick only, and the root mean square (rms) roughness should be as low as possible (minimum < 0.5 nm over the area of the cavity beam waist).<sup>[30]</sup> To achieve the desired long optical and spin coherence times for QIT applications, the membrane needs to be virtually free from lattice defects, paramagnetic impurities, and charge traps. This requires an initial removal of the damaged surface layers of the cut and polished starting material.<sup>[31]</sup> To reach

J. Heupel, J. P. Reithmaier, C. Popov  
Institute of Nanostructure Technologies and Analytics (INA)  
Center for Interdisciplinary Nanostructure Science and Technology (CINSaT)

University of Kassel  
Heinrich-Plett-Str. 40, 34132 Kassel, Germany  
E-mail: j.heupel@ina.uni-kassel.de

M. Pallmann, J. Körber, D. Hunger  
Physikalisches Institut  
Karlsruhe Institute for Technology (KIT)  
Wolfgang-Gaede-Str.1, 76131 Karlsruhe, Germany

D. Hunger  
Institute for Quantum Materials and Technologies (IQMT)  
Karlsruhe Institute for Technology  
Hermann-von-Helmholtz-Platz 1, 76344 Eggenstein-Leopoldshafen, Germany

 The ORCID identification number(s) for the author(s) of this article can be found under <https://doi.org/10.1002/pssa.202200465>.

© 2022 The Authors. physica status solidi (a) applications and materials science published by Wiley-VCH GmbH. This is an open access article under the terms of the Creative Commons Attribution-NonCommercial License, which permits use, distribution and reproduction in any medium, provided the original work is properly cited and is not used for commercial purposes.

DOI: 10.1002/pssa.202200465

the low surface roughness and hence to create high-quality membranes, distinct surface defects like pits, dislocations, and grooves originating from the mechanical–chemical Scaife polishing procedure can pose a challenge.<sup>[32]</sup> Additionally, further processing of diamond by, e.g., dry etching procedures can lead to higher roughening of the surface. One significant defect source is the micro-masking effect. Due to particles on the surface, originating from the polishing procedure or sputtered material during the reactive ion etching (RIE) process, holes or etch pits can be formed at the surface.<sup>[33]</sup>

In the current work, we present our optimized approach to fabricate thin SCD membranes with distinct thicknesses from 5  $\mu\text{m}$  down to 500 nm and a low local rms surface roughness of approx. 0.2 nm (on a  $4 \times 4 \mu\text{m}^2$  area). Starting from our findings published before in ref. [30], we make a step forward and give some insight into new aspects established in the course of the work. The importance of the starting material regarding aspects in the structuring process is pointed out, which deserves more attention due to its critical effect on the final quality of the membrane. Furthermore, we highlight here the importance of the cleaning processes before the actual structuring and during the etching to remove efficiently particles, otherwise causing the micro-masking effect and hence further roughening of the surface. In addition, we present etching recipe combinations for planarization of the surface and removal of defects introduced by the polishing procedure. Finally, the quality of the membranes is evaluated by introducing them into a Fabry–Pérot microcavity and evaluating the membrane-induced losses.

## 2. Results and Discussion

### 2.1. Sample Preparation

To fabricate high-quality membranes, the first crucial parameter is the quality of the starting material. Aside from the choice of high purity diamond, minimum optical grade or more preferred electronic grade, the commercially bought double-side polished samples exhibit an initial rms surface roughness of max. 1.0–1.5 nm ( $5 \times 5 \mu\text{m}^2$ ). With higher roughness values of several nm, it proved to be significantly more difficult to get into the desired range of 0.5 nm or better for the fabricated membranes (example is depicted in Figure S1, Supporting Information). Another important point is the sample planarity, since due to cutting procedures and polishing processes, the thin diamond plates can have high thickness variations along the sample area of more than a few microns. This can lead later on to membranes with minor thickness changes (under 200 nm deviations) only on a small area (e.g., 150–200  $\mu\text{m}$   $\varnothing$  for a membrane with 1 mm  $\varnothing$  and 500  $\mu\text{m}$   $\varnothing$  (Figure S2, Supporting Information), as measured with WLI). The SCD plates purchased exhibited a high planarity of  $\approx 1 \mu\text{m}$  thickness deviation along the sample area. As a result, the structured membranes show a larger area without significant thickness deviations (e.g., 500–600  $\mu\text{m}$   $\varnothing$  for a membrane with 1 mm  $\varnothing$ , as measured with WLI (as discussed in the following and demonstrated in Figure 3a). A comparison via WLI measurements and optical micrographs between samples with distinct thickness variations is presented in Figure S1, Supporting Information. Besides fiber-based cavity measurements,

requiring consistent finesse values for larger membrane areas, this becomes also beneficial for membranes intended for the fabrication processes of larger arrays of other photonic elements like photonic crystal slabs (e.g., even etching of all structures).

To avoid micro-masking in the following dry etching procedures for membrane structuring, it is of utmost importance to start with a clean surface. Besides from sputtered material of the substrate or carrier chip in the ICP-RIE reaction chamber, small particles or impurities on the surface, e.g., stemming from the polishing procedure, can induce micro-masking (e.g., nanopillars “grass effect”<sup>[34]</sup> or pit structures).

Cleaning with solvents like acetone or isopropanol was avoided, since in particular with isopropanol remnants of the cleaning solution were found as spots on the surface via AFM measurements. One cleaning cycle consists of first cleaning in a piranha solution bath to remove any organic contaminations and secondly the sample was cleansed within an oxygen plasma asher to remove particles, e.g., metal impurities,<sup>[30]</sup> at the surface and mainly residuals of the cleaning solutions. In Figure 1 optical micrographs and AFM evaluations for an optical grade, the SCD sample is depicted to emphasize the need for several cleaning cycles.

After an initial 1 h long piranha solution bath, a few defects as well as cleaning solution residuals are recognizable (Figure 1 left), they dominate the AFM image (not shown) hindering the evaluation of the diamond surface, but can be removed by an oxygen plasma treatment. However, as visible in the AFM measurement (Figure 1 middle 3D Plot), the surface still features particles, even though the sample looks clean in the optical micrograph. Hence, a second cleaning cycle (piranha acid +  $\text{O}_2$  plasma treatment) is necessary to reduce drastically the number of particles as noticeable in the AFM 3D plot (Figure 1 right). In principle, these cleaning cycles are repeated until the AFM measurements show no significant amount of particles/defects, i.e., only a few particles not larger than 20 nm. Normally, this is the case after 2–3 repetitions. If the sample is not cleaned thoroughly at the beginning, larger particles, which cannot be removed during the etching, can cause severe micro-masking, affecting the quality of the fabricated membrane due to the creation of large etch pits. In Figure S3, Supporting Information, the evaluation of an exemplary general grade membrane is depicted, which was cleaned only once in piranha acid (3:1, 45 min) before the structuring. The pronounced grooves in the surface topography (Figure 1 right 3D Plot) are typical defects caused by mechanical polishing,<sup>[32]</sup> which lead to the mentioned surface roughness in the range of 1.0–1.5 nm for all examined samples.

### 2.2. Processing of SCD to Remove Sub-Surface Damage

To reduce the surface roughness and remove material damaged due to the polishing from both sample sides, respectively, two distinct steps are implemented before the membrane structuring: A planarization process and a strain relief etch.

For the planarization procedure, the smoothening effect from the isotropic  $\text{Ar}/\text{Cl}_2$  chemistry is exploited.<sup>[35]</sup> While the surface is activated by physical bombardment with Ar ions, chemical reactions between carbon and chlorine atoms are facilitated,

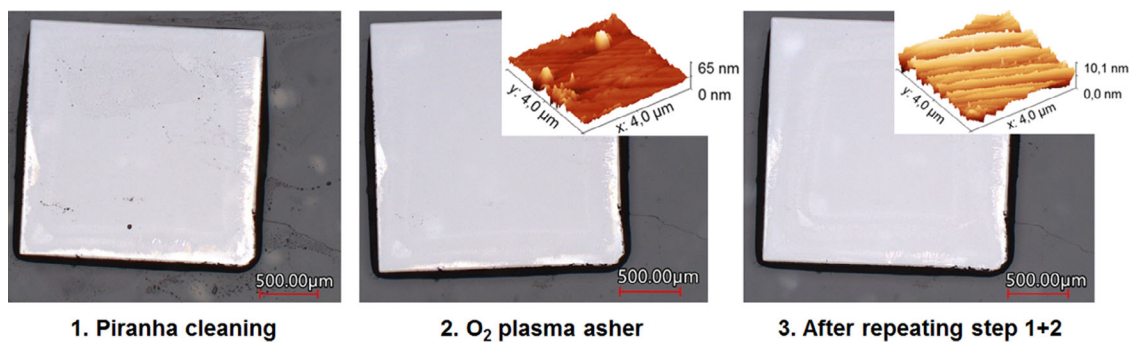


**Figure 1.** Optical micrographs with 3D plots of atomic force microscopy (AFM) measurements as inserts of the same optical-grade single-crystal diamond (SCD) thickness 22–23  $\mu\text{m}$  sample after distinct cleaning procedures: (left) after the first piranha cleaning, (middle) after treatment in an  $\text{O}_2$  plasma asher and (right) after a repetition of cleaning with piranha acid and  $\text{O}_2$  plasma ( $\text{rms} = (1.5 \pm 0.1 \text{ nm})$ ). White parts at the sample edges indicate air inclusions inside the adhesive layer and are not defects at the surface.

forming volatile  $\text{CCl}_x$  products.<sup>[36]</sup> With  $\text{Ar}/\text{Cl}_2$  etch recipes featuring low etch rates, the main aim was to lessen the polishing grooves profile instead of transferring it like it was observed during the later  $\text{O}_2$  structuring steps, where the surface roughness is mainly preserved. The planarization procedure is compromised out of two  $\text{Ar}/\text{Cl}_2$  etching recipes. First, the  $\text{Ar}/\text{Cl}_2$  “standard” recipe, which is as well part of the standard cyclic recipe for the strain relief etch and the later structuring of the membranes. With moderate power values, the etch rate is in a minor range of  $10\text{--}15 \text{ nm min}^{-1}$ , indicating a mild plasma without the capability to deep etch the diamond. The second etching recipe,  $\text{Ar}/\text{Cl}_2$  “soft”, has an even lower etch rate of a few nanometers per minute due to the decreased power values and a low DC bias value ( $\approx 40 \text{ V}$ ). As described in more detail by Radtke et al.,<sup>[37]</sup> with a low or near zero bias value, the acceleration of etching species toward the SCD surface is lowered or even prevented. Therefore, the physical sputtering part of the etching mixture is reduced, while isotropic chemical reactions become more dominant. It is assumed that by a reduced amount of etching species bombardment the SCD surface is less damaged and hence the surface roughness can be further improved. We showed in our previous publication<sup>[30]</sup> that indeed with the

application of the  $\text{Ar}/\text{Cl}_2$  “soft” recipe a reduction of the surface roughness is possible (e.g., from  $\text{rms} \approx 1.2$  to  $0.8 \text{ nm}$  on a  $4 \times 4 \mu\text{m}^2$  area). However, deeper grooves and defects are just transferred instead of being removed. Therefore, different combinations, e.g., also regarding the etch duration, of  $\text{Ar}/\text{Cl}_2$  “standard” and  $\text{Ar}/\text{Cl}_2$  “soft” etch steps were analyzed. In **Figure 2** an AFM evaluation is depicted from the initial surface topography of an optical grade SCD sample after cleaning (Figure 2 left) and then after the planarization procedure, consisting of 20 min  $\text{Ar}/\text{Cl}_2$  “standard” + 30 min  $\text{Ar}/\text{Cl}_2$  “soft” + 20 min  $\text{Ar}/\text{Cl}_2$  “standard” (Figure 2 middle). It is visible that the distinct profile of the polishing grooves is drastically reduced, with a decrease of the  $\text{rms}$  surface roughness from  $\approx 1.3 \text{ nm}$  down to  $0.3 \text{ nm}$  on a  $5 \times 5 \mu\text{m}^2$  area. Additionally, most of the grooves merged and the max. height decreased from 8 to  $2.2 \text{ nm}$ , respectively. With this chosen etch duration  $\approx 700 \text{ nm}$  of material is removed, which is done mainly during the  $\text{Ar}/\text{Cl}_2$  “standard” steps due to a higher etch rate. With shorter durations, this significant effect of the surface roughness reduction was not observed. Furthermore, it seems beneficial to end the planarization process with an  $\text{Ar}/\text{Cl}_2$  “standard” step. Small particles (height of  $2\text{--}3 \text{ nm}$ ) observed on the surface in some cases were

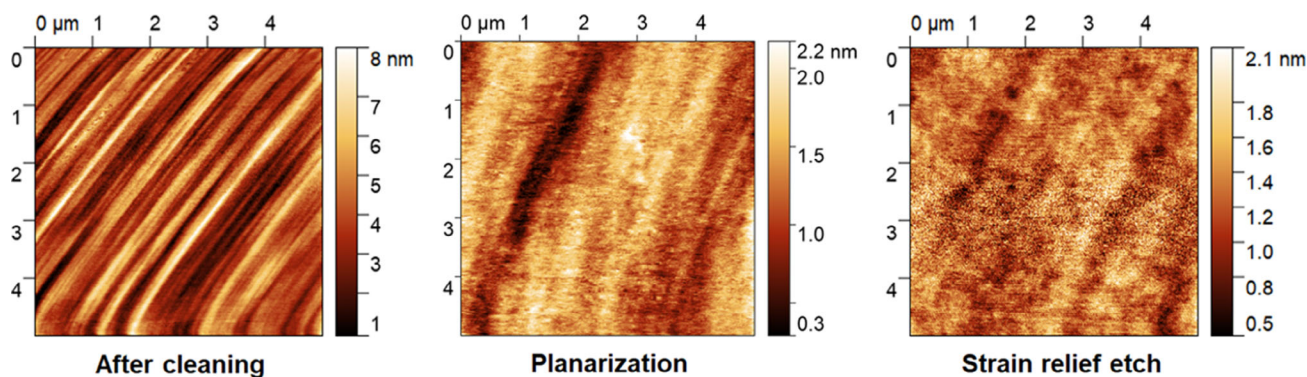


**Figure 2.** AFM measurements of the same optical grade SCD sample after distinct etching procedures: (left) initial surface after cleaning ( $\text{rms} = (1.3 \pm 0.1 \text{ nm})$ ), (middle) after planarization (20 min  $\text{Ar}/\text{Cl}_2$  “standard” + 30 min  $\text{Ar}/\text{Cl}_2$  “soft” + 20 min  $\text{Ar}/\text{Cl}_2$  “standard”, etch depth  $\approx 700 \text{ nm}$ ) the surface roughness is drastically reduced ( $\text{rms} = (0.33 \pm 0.04 \text{ nm})$ ), (right) after strain relief etch with the cyclic  $\text{Ar}/\text{Cl}_2 + \text{O}_2$  recipe (removal of  $\approx 10 \mu\text{m}$ ) sharpness of the polishing grooves is even lessened ( $\text{rms} = (0.26 \pm 0.03 \text{ nm})$ ). The slight bending of the polishing grooves in the left image is due to an AFM artifact.

completely removed with the Ar/Cl<sub>2</sub> “standard” recipe due to more intensive physical sputtering. This low-damage planarization process can be applied to the whole sample area without causing significant defects like etch pits or sputtered particles.

Since polishing damage can extend significantly into the bulk region from hundreds of nanometers up to 10 μm under the surface,<sup>[33,38]</sup> additionally a strain relief etch to remove up to 10 μm is applied on the “bond side” of the sample. For this procedure, a cyclic Ar/Cl<sub>2</sub> + O<sub>2</sub> recipe is utilized. Here the Ar/Cl<sub>2</sub> steps contribute not only to the further smoothening of the surface but also mainly to remove diamond particles that originate from the polishing procedure or are sputtered during the etching, which could cause micro-masking. While the small etch rate of the Ar/Cl<sub>2</sub> steps persists, the O<sub>2</sub> steps are utilized for structuring and hence deep-etching into the diamond with a higher etch rate (≈60 nm min<sup>-1</sup>). The cyclic recipe consists of a long 50 min Ar/Cl<sub>2</sub> “standard” step and then 10 min Ar/Cl<sub>2</sub> “standard” steps in between 15 min long O<sub>2</sub> steps (in total 7x (10 min Ar/Cl<sub>2</sub> + 15 min O<sub>2</sub>) for etching of ≈10 μm). With these Ar/Cl<sub>2</sub> steps in between, particles created during oxygen etching are more efficiently removed to minimize micro-masking and in addition, the smoothening effect is more promoted. This effect is depicted in an AFM measurement on a surface after the planarization procedure (Figure 2 right). While the surface roughness is slightly reduced (from rms ≈0.33 to 0.26 nm), it is evident that micro-masking leading to hole formation was minimized during longer etching processes since no significant defects are visible.

Additionally, only remnants of polishing grooves are left, revealing a planar and clean surface.

### 2.3. Thin SCD Membranes

As elucidated for the strain relief etch, for structuring of SCD membranes the same criteria are valid, i.e., for yielding good quality membranes, the high roughening from the polishing procedure and the micro-masking need to be minimized. Therefore, for the “membrane side” of the sample first the planarization procedure is applied to reduce further the surface roughness.

The thinner the diamond, the more mechanically fragile it becomes; hence one approach is to structure membrane windows (circular or rectangular) instead of etching the whole sample area. Applying diamond bulk masks, different membrane diameters depending on the mask inlets can be fabricated via ICP-RIE. To prevent overetching and hence cracks or trenches toward the membrane edges, the etch masks have angled inlets (74° between front- and backside)

The membranes were structured with the same cyclic Ar/Cl<sub>2</sub> + O<sub>2</sub> recipe as for the strain relief etch. Though, to etch tens of microns to reach the desired thickness of a few micrometers or even less, longer etch durations and hence more etch cycles are necessary.

The first presented membrane (Figure 3a) with a thickness of 600–800 nm and a diameter of 600 μm (total membrane window 1 mm) was fabricated out of a high planarity sample (thickness deviation ≈1 μm over the whole sample). The minor thickness

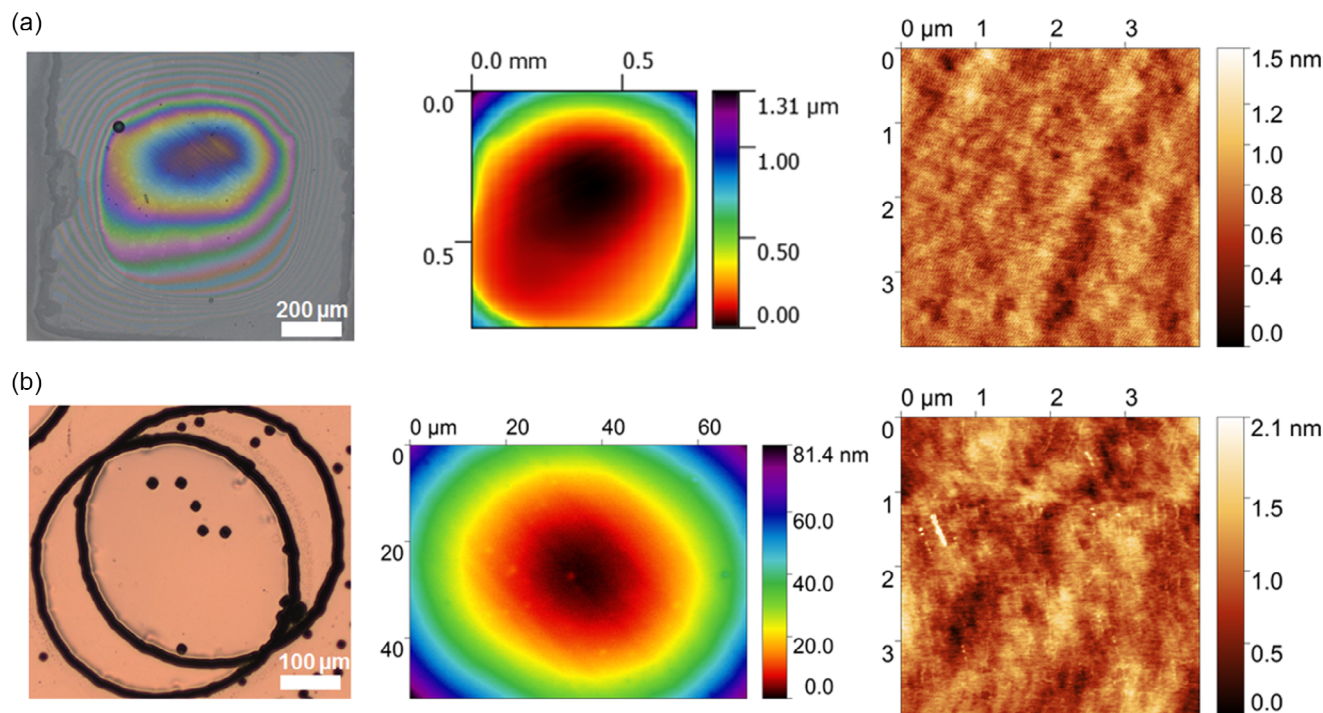


**Figure 3.** Morphological characterization of SCD membranes, from left to the right: overview via optical micrograph, WLI measurement from the membrane center: a) with a 5x Michelson objective and b) with a 50x Mirau objective, AFM image from the center: a) optical grade SCD membrane ( $\varnothing = 600 \mu\text{m}$ , membrane thickness  $\approx 600\text{--}800 \text{ nm}$ , rms =  $(0.19 + 0.05) \text{ nm}$  over a  $4 \times 4 \mu\text{m}^2$ ) out of a high planarity sample (initial thickness 22–23 μm); b) electronic grade SCD membrane ( $\varnothing = 400 \mu\text{m}$ , initial thickness 49–50 μm, membrane thickness  $\approx 3.5\text{--}4 \mu\text{m}$ , rms =  $(0.26 + 0.02) \text{ nm}$  over a  $4 \times 4 \mu\text{m}^2$ ) with shallow NV centers.

deviations of the large membrane area are indicated in a WLI measurement of the membrane center. Due to the planarization procedure and application of the cyclic Ar/Cl<sub>2</sub> + O<sub>2</sub> recipe the rms surface roughness is in the low range of 0.19 nm without any major defects due to, e.g., remnants of polishing grooves or significant micro-masking. Such thinner membranes are more interesting for further incorporation of photonic elements like photonic crystal slabs or free-standing nanobeams. Additionally, it is possible to further tune down the thickness of the membrane by the use of a low etch rate and no damage-inducing Ar/Cl<sub>2</sub> recipes.

Moreover, a further alteration of the fabrication process was analyzed with the depicted electronic grade SCD membrane with a thickness of 3.5–4 μm and a diameter of 400 μm in Figure 3b. Here a sample (1.6 × 1.6 mm<sup>2</sup>) with shallow NV centers with high density, was directly bonded on a dielectric cavity mirror before the membrane structuring. The bond was facilitated via a thin ≈45 nm PMMA layer on the mirror. No further cleaning processes with chemicals, which could deteriorate the bond, were carried out after this procedure. Therefore, a few visible particles were present, which led to micro-masking and formation of holes during the subsequent etching process, as it is visible in the optical micrograph of the membrane. It should be also noted that in this case, about 50 μm was removed by etching. Thus, the long process has widened the holes and resulted in more pronounced features. Additionally, the overlapping membrane edges, indicated on the optical micrograph in Figure 3b, are due to a misalignment of the diamond bulk mask in one of the etch cycles. The mask was not pressed enough on the diamond, hence it shifted during the transfer into the ICP-RIE reaction chamber. Nevertheless, due to the planarization procedure and the membrane structuring recipe, which minimized sub-surface damage from polishing, low rms roughness values of 0.26 nm on a small area scale without any significant defects were achieved. Further AFM measurements, validating the low roughness values at several points on the membrane, are summarized in Figure S4, Supporting Information. Thereby, rms values of ≈0.23 and 0.24 were measured additionally for the membrane

in Figure 3a and 0.27 as well as 0.28 nm for the membrane in Figure 3b.

To confirm the surface quality and show the feasibility for optical applications, we probe the sample inside the cavity and measure the finesse at different spots along a line parallel to a thickness gradient of the membrane, see Figure 4. Coupling the membrane to a resonator leads to a thickness-dependent mode hybridization, which shows an alternating mirror transmission and electric field distribution.<sup>[28,30]</sup> A cavity mode that has an electric field node (antinode) at the diamond–air interface is called “air-like” (“diamond-like”), where most of the stored energy is confined inside the air gap of the cavity (inside the diamond membrane). This also influences the impact of different sources of loss. We expect an increase in scattering and absorption loss for diamond-like modes.

To fit the observed finesse values, we use a model that includes loss by mirror transmission at the fiber ( $\mathcal{L}_f$ ) and planar mirror ( $\mathcal{L}_m$ ), scattering loss at the diamond–air interface ( $\mathcal{L}_{\text{scat}}$ ) and absorption inside the diamond membrane ( $\mathcal{L}_{\text{abs}}$ )<sup>[30]</sup>

$$\mathcal{L}_{\text{eff}} = \frac{2\pi}{\mathcal{F}} = \frac{E_{\text{max,a}}^2}{n_d E_{\text{max,d}}^2} \mathcal{L}_f + \mathcal{L}_m + \mathcal{L}_{\text{scat}}(\sigma_{\text{rms}}) + \mathcal{L}_{\text{abs}}(\alpha_d) \quad (1)$$

The scattering loss depends on the surface roughness  $\sigma_{\text{rms}}$ , given by

$$\mathcal{L}_{\text{scat}} = \sin^2\left(\frac{2\pi n_d t_d}{\lambda_0}\right) \cdot \frac{(1+n_d)(1-n_d)^2}{n_d} \cdot \left(\frac{4\pi\sigma_{\text{rms}}}{\lambda_0}\right)^2 \quad (2)$$

Here,  $t_d$  describes the diamond thickness,  $n_d$  the refractive index of diamond and  $\lambda_0$  the laser wavelength used for the measurement. The absorption loss is given by  $\mathcal{L}_{\text{abs}} \approx 2\beta\alpha_d t_d$ , where  $\alpha_d$  is the absorption coefficient of the diamond. Since absorption only happens inside the diamond membrane, the loss factor is additionally weighted by the ratio of the electromagnetic power inside the diamond to the total intracavity power  $\beta$ . We use the surface roughness and the absorption coefficient as free parameters for the fit. The expected mirror transmission is simulated using a transfer matrix model.

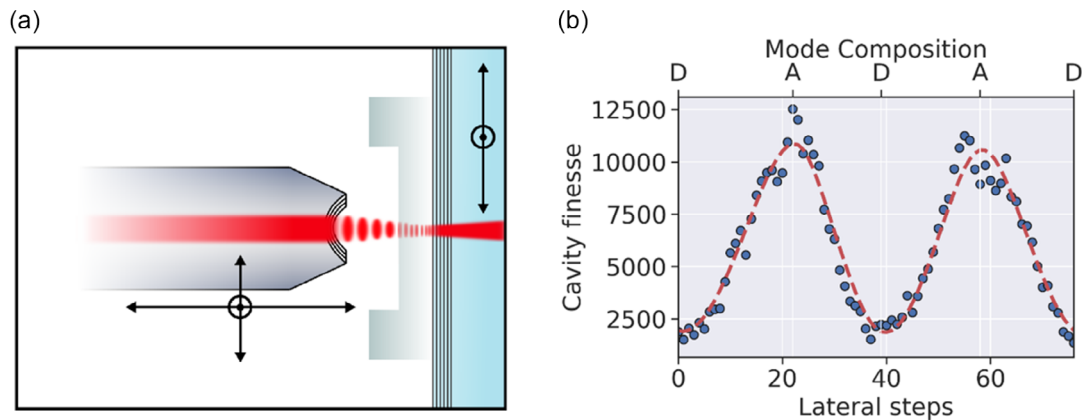


**Figure 4.** Membrane characterization in a fiber-based microcavity. a) Schematic drawing of the cavity setup. The fiber is scanned laterally over the membrane to probe different diamond thicknesses. The full scanning range is up to 100 μm and is chosen such that at least two air-like and diamond-like modes are covered. The transmitted light is recorded on the plane mirror side using an avalanche photodiode (APD). b) Series of finesse measurements for different lateral positions together with a fitted loss model (dashed line).

The measured finesse values are shown in Figure 4b. The discrepancy from the design finesse of 22 000 (4400) for an air-like (diamond-like) mode, as expected from the mirror coatings, can be explained by the sources of loss discussed earlier. The surface roughness extracted from the fit is  $\sigma_{\text{rms}} \approx 0.3$  nm, which is in good agreement with the value obtained from AFM measurements, while the extracted absorption coefficient is  $1.4 \text{ cm}^{-1}$  and thus rather high. This will be discussed in more detail in future work.

### 3. Conclusion

Besides highlighting the importance of the uniformity and initial roughness of the starting SCD material, certain optimizations for the structuring of SCD membranes, especially regarding the removal of surface defects and reduction of the roughness, were presented. First, to prevent micro-masking and hence hole defects during the etching a clean surface is the most crucial component. Therefore, a clean surface before the structuring process is achieved by repeating cleaning cycles with piranha solution (3:1,  $\text{H}_2\text{SO}_4:\text{H}_2\text{O}_2$ ) and cleansing in an oxygen plasma asher. During the distinct etching processes micro-masking needs to be prevented mainly from sputtered and hence redeposited particles during the  $\text{O}_2$  structuring step. To achieve this,  $\text{Ar}/\text{Cl}_2$  cleaning steps were added to the recipe, leading to a final cyclic recipe with alternating  $\text{Ar}/\text{Cl}_2$  and  $\text{O}_2$  steps. We presented several membrane examples, investigated via optical micrographs, WLI measurements, and AFM images, where the micro-masking effect was minimized due to these optimization steps (see also our previous publication<sup>[30]</sup>). To reduce further the surface roughness and thus remove defects like polishing grooves, a planarization procedure was established, consisting of a combination of different  $\text{Ar}/\text{Cl}_2$  recipes with low etch rates ( $\text{Ar}/\text{Cl}_2$  “standard” and  $\text{Ar}/\text{Cl}_2$  “soft”). By exploiting the isotropic  $\text{Ar}/\text{Cl}_2$  chemistry, a significant smoothening effect was achieved, leading together with the cyclic  $\text{Ar}/\text{Cl}_2 + \text{O}_2$  to high-quality SCD membranes with a surface roughness in the range of 0.2 nm on a  $4 \times 4 \mu\text{m}^2$ . This roughness and also the height variation of  $\approx 1.5$  nm (Figure 3a) are targeted for diamond membranes to provide a high finesse in the fiber-based microcavity experiments. Additionally, we presented the fabrication of high planarity membranes with variable geometries and tunable thickness from several microns down to hundreds of nanometers. Therefore, this versatile approach can be customized to distinct applications ranging from  $\mu\text{m}$  thin membranes fabricated directly on cavity mirrors for fiber-based microcavity experiments to thinner membranes intended for other photonic elements like photonic crystal slabs. Besides the versatility, we proved by the presentation of several fabricated membranes the reproducibility of our process.

### 4. Experimental Section

**Fabrication of SCD Membranes:** Different kinds of chemical vapor deposited (CVD) <100> diamond samples with distinctions in purity were used for the structuring of SCD membranes: General grade SCD (Cornes Technologies, USA), optical grade SCD (Applied Diamonds, USA), electronic grade SCD (Applied Diamonds, USA), and electronic grade SCD with incorporated NV centers (Qnami, Switzerland, 70–80 NVs per

$\mu\text{m}^2$  as estimated from confocal measurements, NV depth  $\approx 10$  nm). While the samples' dimensions varied between  $1.5 \times 1.5 \text{ mm}^2$  and  $3 \times 3 \text{ mm}^2$ , the thickness ranged from 20  $\mu\text{m}$  to 50  $\mu\text{m}$  after cutting and thinning via mechanical polishing executed or commissioned by the respective manufacturers. The general grade samples were mainly used for structuring and etch tests. Which kind of single-crystal sample was used is specified by the experimental results.

Based on our previous publication with a detailed description of the SCD membrane fabrication,<sup>[30]</sup> we optimized the structuring process, starting with the mounting of the samples via an adhesive (WaferBOND HT-10.11, Brewer Science, Rolla, MO, USA) on larger quartz glass substrates ( $1 \times 1.2 \text{ cm}^2$ ) for better handling. Afterward, the samples were cleaned with piranha solution (3:1  $\text{H}_2\text{SO}_4:\text{H}_2\text{O}_2$ , 45–60 min) at room temperature and in an oxygen plasma asher (TePla 200-G, 170 W, 0.7 mbar, 3 min). For smoothening of the surface and removal of potentially damaged material and stress induced due to the polishing procedure, a planarization etch process and a strain relief etch<sup>[39]</sup> of several microns were executed in an inductively coupled plasma reactive ion etching (ICP-RIE) system (Oxford Plasmalab 100). The etching recipe for the planarization process consisted out of two distinct  $\text{Ar}/\text{Cl}_2$  recipes: First  $\text{Ar}/\text{Cl}_2$  “standard” (RF power = 200 W, ICP power = 500 W,  $p = 5$  mTorr, Ar flow = 10 sccm,  $\text{Cl}_2$  flow = 20 sccm,  $T_{\text{sub}} = 20^\circ\text{C}$ ) and second  $\text{Ar}/\text{Cl}_2$  “soft”, which features lower values of RF power = 40 W and ICP power = 200 W, so that a low DC bias value of 40 V is achieved. For the strain relief etch the recipe involved alternating  $\text{Ar}/\text{Cl}_2$  (“standard” recipe) and  $\text{O}_2$  (RF power = 90 W, ICP power = 1100 W,  $p = 5$  mTorr,  $\text{O}_2$  flow = 50 sccm,  $T_{\text{sub}} = 20^\circ\text{C}$ ) steps.

Since the samples were polished from both sides, this etching procedure was conducted at first on the later “bond side”, so that the side for bonding on the cavity mirror is clean and smooth. Subsequently, the adhesive was removed (WaferBOND remover), the sample flipped to the other side (“membrane side”) and the mounting and cleaning procedure was repeated. The planarization etch is repeated for the “membrane side” to reduce the initial surface roughness for the following membrane etch. To withstand the long dry etching procedures to reach a final thickness of a few micrometers or less, a bulk diamond mask (Medidia GmbH, Idar-Oberstein, Germany) with angled holes or rectangles ( $74^\circ$  from backside to frontside) was used as an etch mask. The membrane structures were prepared in the ICP-RIE system similar to the strain relief etch with a cyclic recipe consisting of alternating  $\text{Ar}/\text{Cl}_2$  and  $\text{O}_2$  steps with the same elucidated etch parameters. Some further details regarding etch times/etch rates are given for the respective samples in Section 2.2 and 2.3.

**Morphological Characterization of SCD Samples:** Besides an optical evaluation with a white light interferometer (WLI, Zygo New View 5000, Zygo Corporation, Middlefield, CT, USA), the surface topography was investigated using the tapping mode of an atomic force microscope (AFM, DualScope 95, DME, Semilab Germany GmbH, Braunschweig, Germany). The derived data were processed and evaluated with the free-ware Gwyddion version 2.52 (2018). For each surface studied by AFM, 2 or 3 measurements at different points were executed for representation. Hence an error range is added toward the values to indicate variations along the measured surface. Additionally, overview images of the sample and the individual membrane structures were recorded with a confocal laser scanning microscope (Keyence VK-X1000, Keyence Deutschland GmbH, Neu-Isenburg, Germany). To gain more knowledge about the thickness variation along the sample and of the created membrane, again the same WLI was utilized as well as a profilometer (Ambios XP-100, Santa Cruz, CA, USA). For the determination of specific etch rates, either the created etch step, e.g., with the help of the diamond bulk mask edges, or the depth of the hole membrane structure, fabricated with a diamond mask, was analyzed with the same WLI.

**Bonding Procedure and Optical Cavity Characterization:** For the following characterization in a fiber-based microcavity, the adhesive layer between the sample and the substrate was removed. The “bond side” of the SCD membrane sample as well as the planar mirror with dielectric coating were cleaned with piranha solution (2:1  $\text{H}_2\text{SO}_4:\text{H}_2\text{O}_2$ ). The following bonding procedure by van der Waals forces was facilitated via the capillary effect from residual water that remained underneath the diamond sample from the cleaning. To obtain a hydrophilic surface, therefore, the mirror was

cleaned in an oxygen plasma asher (150 W, O<sub>2</sub> = 25 sccm, 5 min) before. Both surfaces were brought into close contact, and the bonding process is finished when all the residual water has evaporated. The bond quality was checked by trying to push the samples with tweezers. A successful van der Waals bond was established when the diamond remains motionless under lateral push (more experimental details can be found in ref. [30]).

The cavity-based measurements were performed in a homebuilt tunable fiber-based Fabry–Pérot scanning microcavity setup.<sup>[40]</sup> It consists of a laterally moveable plane mirror (transmission of 236 ppm <  $T_m$  < 1372 ppm at 637 nm, depending on the local diamond thickness) with the bonded diamond sample and a concave micromirror with a radius of curvature of  $\approx 30 \mu\text{m}$  fabricated on the end facet of a single-mode optical fiber. It is coated with a distributed Bragg reflector (DBR) coating (transmission of  $T_f = 52$  ppm at 637 nm). To probe the cavity, a narrow-linewidth laser (<1 MHz, 639.7 nm) was coupled into the cavity fiber and the transmitted light was detected by an avalanche photodiode (APD). The cavity length was scanned at 10 Hz with a piezo actuator.

## Supporting Information

Supporting Information is available from the Wiley Online Library or from the author.

## Acknowledgements

The authors would like to acknowledge the financial support of the German Federal Ministry of Education and Research (BMBF) under the Project “Quantenrepeater. Link” (QR.X). D.H. acknowledges support from the European Union FETFLAG program, Grant no. 820391 (SQUARE).

Open Access funding enabled and organized by Projekt DEAL.

## Conflict of Interest

The authors declare no conflict of interest.

## Data Availability Statement

The data that support the findings of this study are available from the corresponding author upon reasonable request.

## Keywords

etching, membranes, micro-masking, polishing damage, roughness reduction, single-crystal diamond

Received: July 8, 2022

Revised: October 6, 2022

Published online: December 11, 2022

- [1] A. H. Piracha, P. Rath, K. Ganesan, S. Kühn, W. H. P. Pernice, S. Prawer, *Nano Lett.* **2016**, *16*, 3341.
- [2] A. Trycz, B. Regan, M. Kianinia, K. Bray, M. Toth, I. Aharonovich, *Opt. Mater. Express* **2019**, *9*, 4708.
- [3] M. Ruf, M. Ijspeert, S. van Dam, N. de Jong, H. van den Berg, G. Evers, R. Hanson, *Nano Lett.* **2019**, *19*, 3987.
- [4] R. P. Mildren, J. R. Rabeau, *Optical Engineering of Diamond*, Wiley-VCH Verlag GmbH & Co. KGaA, Weinheim, Germany **2013**.
- [5] I. Aharonovich, A. D. Greentree, S. Prawer, *Nat. Photon* **2011**, *5*, 397.
- [6] C. Delfaure, M. Pomorski, J. de Sanoit, P. Bergonzo, S. Saada, *Appl. Phys. Lett.* **2016**, *108*, 252105.

- [7] S. Ghosh, H. Surdi, F. Kargar, F. A. Koeck, S. Rumyantsev, S. Goodnick, R. J. Nemanich, A. A. Balandin, *Appl. Phys. Lett.* **2022**, *120*, 62103.
- [8] S. Mi, M. Kiss, T. Graziosi, N. Quack, *J. Phys. Photonics* **2020**, *2*, 42001.
- [9] H. Liu, M. Wang, P. Yu, X. Ye, S. Shi, P. Wang, F. Shi, Y. Wang, J. Du, in *Symp. Latsis 2019 on Diamond Photonics - Physics, Technologies and Applications*, OSA, Washington, DC, p. 90.
- [10] B. Regan, S. Kim, A. T. H. Ly, A. Trycz, K. Bray, K. Ganesan, M. Toth, I. Aharonovich, *InfoMat* **2020**, *2*, 1241.
- [11] M. H. Abobeih, J. Cramer, M. A. Bakker, N. Kalb, M. Markham, D. J. Twitchen, T. H. Taminiau, *Nat. Commun.* **2018**, *9*, 2552.
- [12] D. D. Sukachev, A. Sipahigil, C. T. Nguyen, M. K. Bhaskar, R. E. Evans, F. Jelezko, M. D. Lukin, *Phys. Rev. Lett.* **2017**, *119*, 223602.
- [13] M. K. Bhaskar, R. Riedinger, B. Machielse, D. S. Levonian, C. T. Nguyen, E. N. Knall, H. Park, D. Englund, M. Lončar, D. D. Sukachev, M. D. Lukin, *Nature* **2020**, *580*, 60.
- [14] K. Nemoto, M. Trupke, S. J. Devitt, A. M. Stephens, B. Scharfenberger, K. Buczak, T. Nöbauer, M. S. Everitt, J. Schmiedmayer, W. J. Munro, *Phys. Rev. X* **2014**, *4*, 031022.
- [15] R. Albrecht, A. Bommer, C. Deutsch, J. Reichel, C. Becher, *Phys. Rev. Lett.* **2013**, *110*, 243602.
- [16] L. Childress, R. Hanson, *MRS Bull.* **2013**, *38*, 134.
- [17] J. N. Becker, C. Becher, *Phys. Status Solidi A* **2017**, *214*, 1700586.
- [18] S. Häußler, J. Benedikter, K. Bray, B. Regan, A. Dietrich, J. Twamley, I. Aharonovich, D. Hunger, A. Kubanek, *Phys. Rev. B* **2019**, *99*, 165310.
- [19] P. Siyushev, F. Kaiser, V. Jacques, I. Gerhardt, S. Bischof, H. Fedder, J. Dodson, M. Markham, D. Twitchen, F. Jelezko, J. Wrachtrup, *Appl. Phys. Lett.* **2010**, *97*, 241902.
- [20] N. Felgen, B. Naydenov, F. Jelezko, J. P. Reithmaier, C. Popov, *Phys. Status Solidi A* **2018**, *215*, 1800371.
- [21] E. Neu, P. Appel, M. Ganzhorn, J. Miguel-Sánchez, M. Lesik, V. Mille, V. Jacques, A. Tallaire, J. Achard, P. Maletinsky, *Appl. Phys. Lett.* **2014**, *104*, 153108.
- [22] L. Marsegli, J. P. Hadden, A. C. Stanley-Clarke, J. P. Harrison, B. Patton, Y.-L. D. Ho, B. Naydenov, F. Jelezko, J. Meijer, P. R. Dolan, J. M. Smith, J. G. Rarity, J. L. O'Brien, *Appl. Phys. Lett.* **2011**, *98*, 133107.
- [23] M. Jamali, I. Gerhardt, M. Rezai, K. Frenner, H. Fedder, J. Wrachtrup, *Rev. Sci. Instrum.* **2014**, *85*, 123703.
- [24] T. Schröder, M. Walsh, J. Zheng, S. Mouradian, L. Li, G. Malladi, H. Bakhru, M. Lu, A. Stein, M. Heuck, D. Englund, *Opt. Mater. Express* **2017**, *7*, 1514.
- [25] J. Riedrich-Möller, C. Arend, C. Pauly, F. Mücklich, M. Fischer, S. Gsell, M. Schreck, C. Becher, *Nano Lett.* **2014**, *14*, 5281.
- [26] D. Hunger, T. Steinmetz, Y. Colombe, C. Deutsch, T. W. Hänsch, J. Reichel, *New J. Phys.* **2010**, *12*, 65038.
- [27] E. Janitz, M. Ruf, M. Dimock, A. Bourassa, J. Sankey, L. Childress, *Phys. Rev. A* **2015**, *92*, 043844.
- [28] H. Kaupp, T. Hümmer, M. Mader, B. Schlederer, J. Benedikter, P. Haeusser, H.-C. Chang, H. Fedder, T. W. Hänsch, D. Hunger, *Phys. Rev. Appl.* **2016**, *6*, 054010.
- [29] S. B. van Dam, M. Ruf, R. Hanson, *New J. Phys.* **2018**, *20*, 115004.
- [30] J. Heupel, M. Pallmann, J. Körber, R. Merz, M. Kopnarski, R. Stöhr, J. P. Reithmaier, D. Hunger, C. Popov, *Micromachines* **2020**, *11*, 1080.
- [31] P. Appel, E. Neu, M. Ganzhorn, A. Barfuss, M. Batzer, M. Gratz, A. Tschöpe, P. Maletinsky, *Rev. Sci. Instrum.* **2016**, *87*, 63703.
- [32] M.-L. Hicks, A. C. Pakpour-Tabrizi, V. Zuerbig, L. Kirste, C. Nebel, R. B. Jackman, *J. Appl. Phys.* **2019**, *125*, 244502.
- [33] M.-L. Hicks, A. C. Pakpour-Tabrizi, R. B. Jackman, *Diamond Relat. Mater.* **2019**, *97*, 107424.
- [34] Y. Ando, Y. Nishibayashi, K. Kobashi, T. Hirao, K. Oura, *Diamond Relat. Mater.* **2002**, *11*, 824.

- [35] C. L. Lee, E. Gu, M. D. Dawson, I. Friel, G. A. Scarsbrook, *Diamond Relat. Mater.* **2008**, *17*, 1292.
- [36] A. Toros, M. Kiss, T. Graziosi, S. Mi, R. Berrazouane, M. Naamoun, J. Vukajlovic Plestina, P. Gallo, N. Quack, *Diamond Relat. Mater.* **2020**, *108*, 107839.
- [37] M. Radtke, L. Render, R. Nelz, E. Neu, *Opt. Mater. Express* **2019**, *9*, 4716.
- [38] P.-N. Volpe, P. Muret, F. Omnes, J. Achard, F. Silva, O. Brinza, A. Gicquel, *Diamond Relat. Mater.* **2009**, *18*, 1205.
- [39] L. Xie, T. X. Zhou, R. J. Stöhr, A. Yacoby, *Adv. Mater.* **2018**, *30*, 1705501.
- [40] B. Casabone, J. Benedikter, T. Hümmer, F. Oehl, K. D. O. Lima, T. W. Hänsch, A. Ferrier, P. Goldner, H. D. Riedmatten, D. Hunger, *New J. Phys.* **2018**, *20*, 95006.